Nanosails Showcasing Zn_3As_2 as an Optoelectronic-Grade Earth Abundant Semiconductor

*Elias Z. Stutz, Martin Friedl, Tim Burgess, Hark Hoe Tan, Philippe Caroff, Chennupati Jagadish, and Anna Fontcuberta i Morral**

Zn_3As_2 is a promising earth-abundant semiconductor material. Its bandgap, around 1 eV, can be tuned across the infrared by alloying and makes this material suited for applications in optoelectronics. Here, we report the crystalline structure and electrical properties of strain-free Zn_3As_2 nanosails, grown by metal-organic vapor phase epitaxy. We demonstrate that the crystalline structure is consistent with the $P4_2/nmc$ (D_{4h}^{15}) α"-Zn_3As_2 metastable phase. Temperature-dependent Hall effect measurements indicate that the material is degenerately p-doped with a hole mobility close to $10^3\,cm^2\,V^{-1}\,s^{-1}$. Our results display the potential of Zn_3As_2 nanostructures for next generation energy harvesting and optoelectronic devices.

The increasing production of high-performance electronic devices and the push towards generating energy in a sustainable manner leads to sustainability challenges for optoelectronic and photovoltaic (PV) technologies. Particularly affected are devices using atomic elements of scarce abundance in the earth's crust, which prevents their widespread deployment. In this context, highly functional materials made of earth-abundant elements are being sought for both PV and optoelectronic applications. The second most abundant element in the earth's crust, silicon, is a semiconductor very successfully deployed in the PV market. It suffers nonetheless from its indirect bandgap and the consequently high purity required for the production of efficient solar cells. Both characteristics increase the energy needs for silicon PV device production. The so-called "second generation" solar cells, built with much thinner, direct bandgap active layers, could in principle solve these two issues. Still, these thin film solar cells exhibit either a long energy payback time (amorphous silicon) or they use scarce and expensive elements (ex: copper, indium, gallium, selenium, cadmium, tellurium).

Direct bandgap semiconductors employing earth-abundant elements could combine the advantages of all these material families. They would enable efficient light collection in a thin film of easily available materials. Copper zinc tin sulfide (CZTS) and zinc phosphide (Zn_3P_2) have received increasing attention as materials satisfying these criteria for efficient and sustainable light conversion discussed so far. Belonging to the same family, zinc arsenide (Zn_3As_2) is a p-type semiconductor structurally similar to Zn_3P_2. It exhibits a band gap around 1.0 eV[1] and potentially high hole mobilities.[2] The stoichiometry of this material can be transformed continuously into Cd_3As_2[3] or Zn_3P_2[4] by appropriate atomic substitutions, shifting its bandgap energy toward 1.5 eV and 0 eV, respectively. $(Zn_{1-x}Cd_x)_3As_2$ transforms from a semiconductor to a three-dimensional Dirac semimetal as x reaches 0.62.[5] The ability to tune its direct bandgap energy makes this material system very attractive for long-wavelength optoelectronics and as a constituent in multi-junction solar cells.

$M_3^{II}X_2^V$ compounds crystallize in a structure akin to the anti-fluorite structure, with the difference being that 25% of the cation sites are empty. In turn, this causes a slight tetragonal distortion. Barring the minute deformation, their anion sublattice is face-centered cubic. Historically, the progress in the use of II–V materials has been hindered by a lack of suitable substrates matched in terms of their lattice constants and large coefficient of thermal expansion (CTE). InP and GaAs have shown to be the most suited substrates for the growth of Zn_3As_2, with lattice mismatches of 0.35% and 4% at 300K, respectively.[6] One should note here however that using InP and GaAs defies the purpose of achieving a sustainable technology with earth-abundant elements. Epitaxial thin films of Zn_3As_2 have been obtained by metal-organic vapor phase epitaxy,[7] molecular beam epitaxy,[8] and liquid phase epitaxy.[9] In all these reports, misfit dislocations and cracks at the interface of thin films seem to be unavoidable.[10] The resulting interface defects drastically impair the electrical properties of the heterostructures.

One solution to both the lattice mismatch and CTE difference problems constitutes the use of freestanding nanostructures rather than thin films. In this case, the nanoscale contact area with the substrate allows for very efficient elastic strain relaxation.[11] Examples of heterogeneous integration of

E. Z. Stutz, M. Friedl, Prof. A. Fontcuberta i Morral
Laboratoire des Matériaux Semiconducteurs
École Polytechnique Fédérale de Lausanne, EPFL
1015 Lausanne, Switzerland
E-mail: anna.fontcuberta-morral@epfl.ch

Dr. T. Burgess, Prof. H. H. Tan, Dr. P. Caroff, Prof. C. Jagadish
Department of Electronic Materials Engineering
Research School of Physics and Engineering
The Australian National University
Canberra, ACT 2601, Australia

Prof. A. Fontcuberta i Morral
Institute of Physics, School of Basic Sciences
École Polytechnique Fédérale de Lausanne, EPFL
1015 Lausanne, Switzerland

DOI: 10.1002/pssr.201900084

materials in the form of nanoparticles or nanowires are numerous.[12–15] Until now there are only a few publications demonstrating synthesis of Zn_3As_2 and Zn_3P_2 nanostructures,[2,16–18] including simple device demonstration such as field-effect transistors and photodetectors.[2]

Other kinds of free-standing structures include two-dimensional nanoscale objects such as nanosails or nanoscale membranes.[19–22] Thanks to their potentially equally efficient relaxation of mismatch strain, they provide a perfect platform for the study of two-dimensional structures which are free from any dislocations or cracks. They thus provide information on the intrinsic properties of the material and a path for their realistic use in applications.

Experimental Details: The Zn_3As_2 nanosails were grown by horizontal flow gold-catalyzed metal-organic vapor phase epitaxy (MOVPE) on a GaAs (111)B substrate by the vapor-liquid-solid method, as in ref. [18]. The growth time was 10 min. Details of the growth are described in the supplementary information. The morphological properties of the nanosails were characterized by scanning electron microscopy (SEM) and by atomic force microscopy (AFM). **Figure 1** shows a typical SEM picture of the as-grown sample.

Micro-Raman scattering measurements were performed on individual nanosails at 12 K with a single-frequency optically pumped semiconductor laser at 532 nm wavelength as an excitation source. The laser, with a power of 140 μW at the sample surface, was focused on the sample with a microscope objective (NA = 0.75). The polarization of the incident laser was controlled by a linear polarizer. The scattered light was collected in backscattering geometry through the same objective and recorded by a TriVista triple spectrometer with gratings of 900, 900, and 1800 lines mm^{-1}, respectively, and a Princeton Instruments liquid nitrogen cooled multichannel CCD PyLoN camera.

For the device fabrication, the nanosails were detached from the growth substrate by sonication in isopropanol and drop cast onto a thermally oxidized silicon wafer. The contacts were then patterned with aligned e-beam lithography[23] followed by wet etching in a buffered hydrogen fluoride solution with one chip additionally being Ar milled in-situ before metal deposition (see supplementary information for details). The contacts were then deposited by sputtering 20 nm of Cr and 150 nm of Au. The conductivity of the nanosails was measured by applying the van der Pauw method[24] while the thickness of the nanostructures was determined by AFM. The Hall mobility of the nanostructures was measured employing the same four contacts while sweeping a perpendicular magnetic field from −5 T to 5 T.

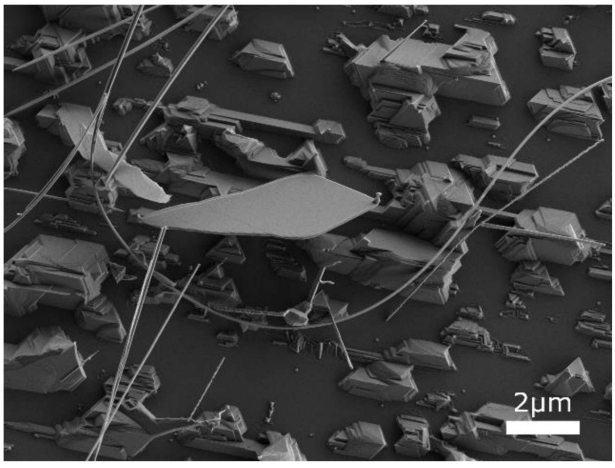

Figure 1. Typical top-view scanning electron microscopy image of the surface of a sample grown in the conditions described in the text. Nanosails, nanowires, and gold nanoparticles can be seen.

Structural Properties: We start by reporting the structural properties of the nanosails. In bulk form, pure Zn_3As_2 exists in three different polymorphs named α, α', and β.[25] This material can also be found in a fourth crystalline structure when 2–4% of zinc or arsenic atoms are substituted with cadmium[26] or phosphorus,[27] respectively. **Table 1** lists the four polymorphs along with their characteristics in terms of symmetry, stability, and number of atoms in the unit cell.

The thermodynamically stable Zn_3As_2 phase at room temperature is the so-called α phase. At temperatures between 457 and 945 K, typically used for growth, the α' phase with a different symmetry becomes stable. At higher temperatures, the β phase becomes stable. The loss of order of the cations increases the symmetry of this phase and makes it face-centered cubic. Pangilinan et al.[28] have observed a strained phase whose symmetry could not be matched with any known pure phase of Zn_3As_2. They have not identified it as such at that time but given that the symmetry of their phase matches that of the α" phase, this is the first observation of stoichiometrically pure α"-Zn_3As_2. To the best of our knowledge, this phase has otherwise never been synthesized and identified before.

Raman spectroscopy is a non-destructive technique that provides information not only on the structure, but also on the orientation and symmetry of the material. **Figure 2** shows a representative Raman spectrum of a Zn_3As_2 nanosail. The spectrum exhibits a dozen peaks separated in two sets: one at low energy ascribed to bending vibrations of the X-Zn-X systems (X = As, P) and the other at high energy, attributed to fundamental stretching vibrations of the Zn-X bonds.[29] The exact position of the deconvoluted stretching mode peaks along with their symmetry are reported in **Table 2**. The bending mode peaks acquired under our measurement conditions overlap too much to be reliably deconvoluted. One peak (*) could be the reportedly anomalous peak also observed by Pangilinan.[28] A similar Raman spectrum to the one presented here is observed in α- or α" Zn_3P_2,[30] another compound of the α"-$(Zn_{1-x}Cd_x)_3(P_{1-y}As_y)_2$ quaternary phase. This structure of the Raman spectrum is not observed in a lower symmetry phase of Zn_3As_2 such as α.[31] The Raman shift of the peaks identified in that article are listed in Table S1 in the supplementary information for comparison.

Table 1. The different observed phases of Zn_3As_2, their space group, stability in the bulk and number of atoms in the unit cell.

Name	Space group	Stability in bulk	# of atoms
α	$I4_1cd$	Stable: ≈300K	160
α'	$P4_2/nbc$	Stable: 457–945 K	160
β	$Fm\bar{3}m$	Stable: >945 K	10
α"	$P4_2/nmc$	Metastable	40

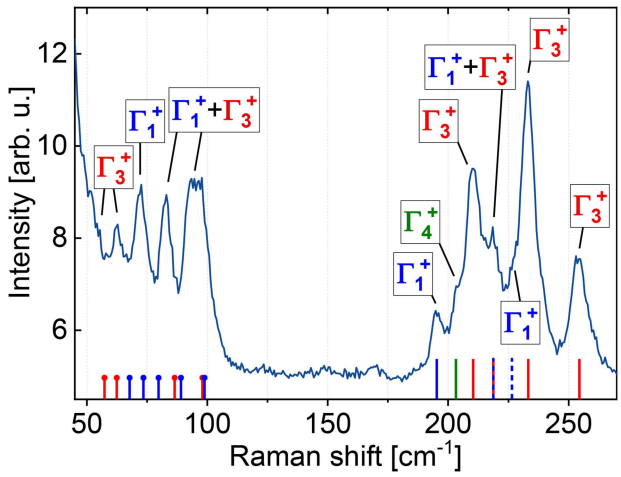

Figure 2. Raman spectrum of a nanosail acquired at 12 K in backscattering geometry. The incident 532 nm laser light at approx. 150 μW was linearly polarized along the main axis of the nanostructure while the scattered light was unpolarized.

In a previous study, Burgess et al.[18] assigned the α' phase of Zn_3As_2 to the nanosails obtained in extremely similar conditions (400 °C on GaAs(110)). The crystal structure was assigned by comparing electron diffraction patterns to simulated diffraction patterns of the α- and α'-Zn_3As_2 structures, and the latter seemed to be the most suitable. We simulated the diffraction pattern of α"-Zn_3As_2 in equivalent zone axes to compare with their experimental diffraction patterns. The zinc ordering in the α" phase does not match the crystalline structure of their nanostructures. Details of the simulation are shown in the supplementary information.

Prior to the growth described here, the MOCVD system had been used to grow zinc phosphide on indium phosphide substrates. It is possible that there was some residual phosphorus originating from the precursor or from the substrate in the growth chamber which could have been incorporated in the nanosails. This would explain the growth of the α" phase.[27]

Further evidence indicating that our nanosails belong to this phase is that the crystal structure exhibits a relatively small unit cell with 40 atoms, four times less than the α and α' phases. This is consistent with the reduced number of observed first-order phonons in our structures.

In conclusion, Raman spectra are consistent with the crystalline phase of the nanosails being α"-Zn_3As_2.

Electrical Properties: **Figure 3**a shows a nanosail device, with its four electrical contacts. The thickness of the characterized devices, determined with AFM, ranged from 80 to 160 nm.

We start by reporting on the temperature dependence of the electrical conductivity, between 4 and 300 K. The measurements of three different nanosails obtained in the same batch are shown in Figure 3b. The conductivity increases at lower temperatures. Such a behavior is only expected in metals or in semiconductors with degenerate doping.

Figure 4a shows an example of a typical relationship between the measured Hall voltage and the applied magnetic field. The positive slope of the curves indicates a positive Hall coefficient, and hence confirms that the material is p-type, as reported extensively in the literature. The data follows the linear dependence of the Hall voltage as a function of the magnetic field: $V_H = \frac{IB}{pte}$ with a regression close to 1 ($\rho^2 = 0.9997$).

We use the conductivity measurements and the Hall voltage to determine the carrier concentration and mobility as a function of temperature. The concentration of free carriers and mobility is shown in Figure 4b,c, respectively. The carrier concentration

Table 2. Deconvoluted peak positions of the high Raman shift stretching modes obtained by fitting with Lorentzians.

Position	Mode representation	Position in [28]
195.3	Γ_1^+	196.7
203.2	Γ_4^+	204.9
210.3	Γ_3^+	210.6
218.8	Γ_1^+ & Γ_3^+	215.4
226.5	Γ_1^+ (*)	225.7
233.2	Γ_3^+	232.4
254.5	Γ_3^+	252.1

The peak positions are matched with the corresponding peak and their symmetry determined by Pangilinan et al.[28]

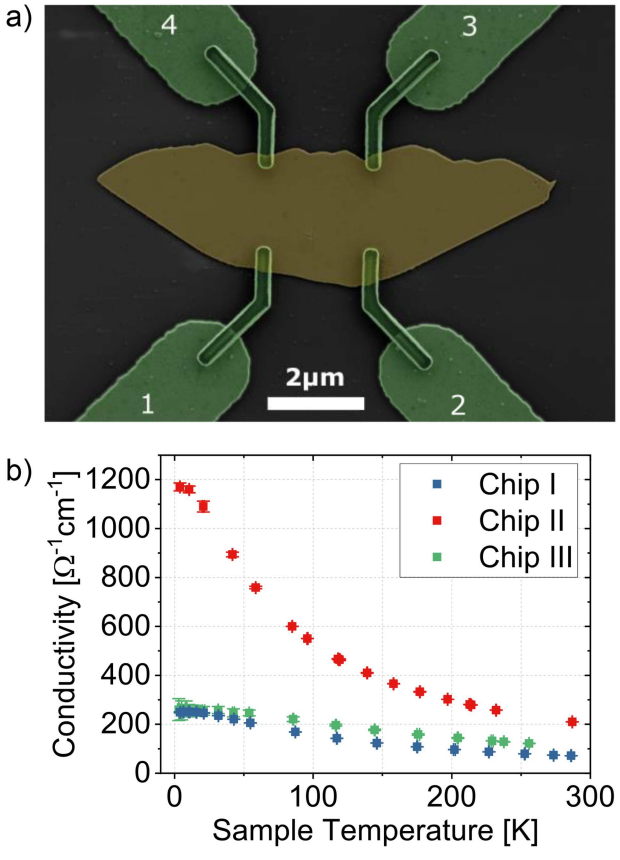

Figure 3. a) Top-view colorized SEM image of a Zn_3As_2 nanosail (yellow) and the four contacts used for electrical characterization (green). b) Evolution of the conductivity of three nanosails with temperature, measured with the van der Pauw method.

increases at high temperatures but does not freeze out at low temperatures, remaining above $4\times10^{18}\,cm^{-3}$.

In all nanosails studied, the mobility of the carriers is constant below 10 K and decreases at higher temperatures. Linear fits to the high-energy parts of the curves reveal that the mobility is nearly proportional to the inverse of the temperature. This dependence is typical of metals and degenerate semiconductors, for which lattice vibrations are the dominant sources of scattering above their Debye temperature.

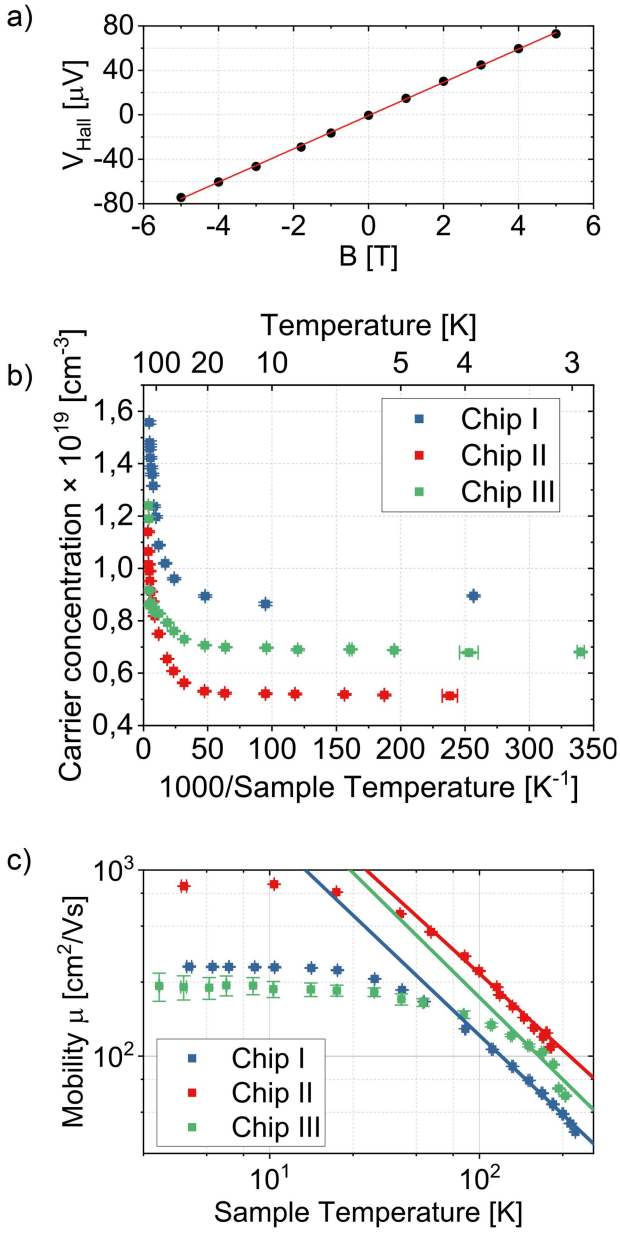

Figure 4. a) Variation of the Hall voltage with magnetic field applied on to the nanosail and (in red) a linear fit to the data. b) temperature dependence of the carrier concentration of three nanosails calculated using the measured Hall coefficients and c) evolution of the hole mobility with the temperature (points). A fit to the linear high-temperature regime (solid lines) provides the temperature dependence of lattice scattering in Zn_3As_2.

The three nanosails characterized have qualitatively very similar properties. The most striking difference between the three is the approximately threefold increase in carrier mobility measured in Chip II with respect to the other two. This in turn could explain most of the 4.5-fold increase in conductivity in that same nanosail. The reasons why this nanostructure exhibits increased mobility and conductivity with respect to the other two could be due to local differences of the growth conditions and environment during growth.

Overall, the electrical measurements indicate that the Zn_3As_2 nanosails are degenerately doped. Our results are consistent with some of the prior works on epitaxial Zn_3As_2.[1,6,32,33] The Zn_3As_2 material in this study is found to be unintentionally p-type. The unintentional p-doping is attributed to shallow[8] native defects.[34] Acceptor levels within a few dozen meV from the valence band maximum (VBM) have been detected in Zn_3As_2 by electrical, absorption,[33] and photoluminescence,[7,35] spectroscopy measurements. Using the tight-binding method, Szatkowski et al. calculated the energy levels of vacancies.[36] They determined that zinc vacancies induce levels within 20 meV of the VBM. These findings are supported by Density-Functional Theory (DFT) computations of the point defect energy levels of Zn_3P_2,[37] which exhibits the same short-range order as Zn_3As_2. Finally, the presence of an impurity band (IB) in Zn_3As_2 due to the degenerate doping was proposed by Iwami et al.[32] and Sujak-Cyrul et al.[33]

The temperature dependence of the carrier concentration of our nanosails also shows two different regimes: below about 30 K, the concentration is nearly constant, and at higher temperatures, or only until about 80 K in Chip III, the concentration increases considerably. The transition temperature has been obtained by fitting the two regimes, as shown in Figure S2 in the Supporting Information information. The constant low-temperature regime indicates that pure impurity band conduction occurs up to these temperatures, at which point thermal carrier generation initiates, leading to a further increase of the carrier concentration. The spacing between the VBM and the IB has been determined from the onset of thermal carrier generation to be 2.5 meV, a value consistent with previous observations. Whether the IB carrying the conduction carriers at the lowest temperature is degenerate with the top of the valence band or separated from it remains to be determined.

Based on the literature describing the low-temperature carrier properties of Zn_3As_2, the presence of an IB seems to be ubiquitous in this kind of material, whether synthesized by the Bridgman method,[32] by resublimation,[33] or pseudomorphically on InP by MBE.[6]

Comparison of the conductivities measured in the different works shows striking differences. For example, Szatkowski obtained $7\,\Omega^{-1}\,cm^{-1}$ at 5 K, Sujak-Cyrul $35\,\Omega^{-1}\,cm^{-1}$ (calc.) at 5 K and Chelluri $220\,\Omega^{-1}\,cm^{-1}$ (calc.) at 10 K. This is to be compared with our results of at least $250\,\Omega^{-1}\,cm^{-1}$ at 5 K. Szatkowski et al., reporting the lowest measured conductivity in single crystals at 5 K. This might be due to the presence of a higher density of defects associated with the growth method. Similarly, a reduction of the carrier mobility in Zn_3As_2 thin films with decreasing material quality has been reported by Kolodka.[38]

Overall, the high values of mobility obtained by in this work indicates the high potential of nanosails to investigate the intrinsic properties of materials bypassing lattice constant and CTE mismatch challenges. In addition, we believe our results show Zn_3As_2 has excellent potential for photovoltaic applications. For this to be possible, junctions should be created by also growing n-type regions or by heteroepitaxy of a second material yielding a type-II band alignment. Further work could also aim at optimizing the growth conditions to increase the yield of nanosails as in refs. [39–40].

In conclusion, we have shed light on the electrical properties of α"-Zn_3As_2 nanosails, whose crystalline structure has been demonstrated by polarized Raman spectroscopy. The temperature dependence of the conductivity, majority carrier concentration and carrier mobility between 4 and 300 K are consistent with a high-quality degenerately doped p-type semiconductor. This work demonstrates the potential of Zn_3As_2 as an earth-abundant semiconductor for next generation energy harvesting or optoelectronic applications.

Acknowledgements

EZS and MF have contributed equally to this work. MF, EZS, and AFiM thank financial support by SNSF through the QSIT network and consolidator grant Easeh (grant nr BSCGI0_157705), as well as initial discussions with Andreana Daniil and Simon Escobar Steinvall. We acknowledge the Australian National Fabrication Facility, ACT Node for access to the MOCVD facility.

Conflict of Interest

The authors declare no conflict of interest.

Keywords

II–V compounds, degenerate semiconductors, earth abundant materials, Hall effect, nanosails, optoelectronics, zinc arsenide

Received: February 11, 2019
Revised: March 1, 2019
Published online:

[1] J. Szatkowski, K. Sierański, *J. Phys. Chem. Solids* **1990**, *51*, 249.
[2] G. Chen, Z. Liu, B. Liang, G. Yu, Z. Xie, H. Huang, B. Liu, X. Wang, D. Chen, M.-Q. Zhu, G. Shen, *Adv. Funct. Mater.* **2013**, *23*, 2681.
[3] G. A. Castellion, L. C. Beegle, *J. Phys. Chem. Solids* **1965**, *26*, 767.
[4] H. S. Im, K. Park, D. M. Jang, C. S. Jung, J. Park, S. J. Yoo, J.-G. Kim, *Nano Lett.* **2015**, *15*, 990.
[5] H. Lu, X. Zhang, Y. Bian, S. Jia, *Sci. Rep.* **2017**, *7*, 1.
[6] B. Chelluri, T. Y. Chang, A. Ourmazd, A. H. Dayem, J. L. Zyskind, A. Srivastava, *J. Cryst. Growth* **1987**, *81*, 530.
[7] J. R. Botha, G. J. Scriven, J. A. A. Engelbrecht, A. W. R. Leitch, *J. Appl. Phys.* **1999**, *86*, 5614.
[8] B. Chelluri, T. Y. Chang, A. Ourmazd, A. H. Dayem, J. L. Zyskind, A. Srivastava, *Appl. Phys. Lett.* **1986**, *49*, 1665.
[9] S. Sudhakar, V. Ganesh, I. Sulania, P. K. Kulriya, K. Baskar, *J. Phys. D: Appl. Phys.* **2007**, *40*, 5071.
[10] J. A. A. Engelbrecht, G. J. Scriven, J. H. Neethling, M. C. Wagener, *J. Cryst. Growth* **2000**, *216*, 235.
[11] F. Glas, *Phys. Rev. B — Condens. Matter Mater. Phys.* **2006**, *74*, 121302.
[12] M. T. Björk, B. J. Ohlsson, T. Sass, A. I. Persson, C. Thelander, M. H. Magnusson, K. Deppert, L. R. Wallenberg, L. Samuelson, *Nano Lett.* **2002**, *2*, 87.
[13] M. Glaser, A. Kitzler, A. Johannes, S. Prucnal, H. Potts, S. Conesa-Boj, L. Filipovic, H. Kosina, W. Skorupa, E. Bertagnolli, C. Ronning, A. Fontcuberta i Morral, A. Lugstein, *Nano Lett.* **2016**, *16*, 3507.
[14] L. C. Chuang, M. Moewe, K. W. Ng, T.-T. D. Tran, S. Crankshaw, R. Chen, W. S. Ko, C. Chang-Hasnain, *Appl. Phys. Lett.* **2011**, *98*, 123101.
[15] K.-W. Kwon, M. Shim, *J. Am. Chem. Soc.* **2005**, *127*, 10269.
[16] N. Kouklin, S. Sen, M. Gajdardziska-Josifovska, *Appl. Phys. Lett.* **2006**, *89*, 071901.
[17] J. Li, L.-S. Wang, D. B. Buchholz, R. P. H. Chang, *Nano Lett.* **2009**, *9*, 1764.
[18] T. Burgess, P. Caroff, Y. Wang, B. H. Badada, H. E. Jackson, L. M. Smith, Y. Guo, H. H. Tan, C. Jagadish, *Nano Lett.* **2015**, *15*, 378.
[19] M. de la Mata, R. Leturcq, S. R. Plissard, C. Rolland, C. Magén, J. Arbiol, P. Caroff, *Nano Lett.* **2016**, *16*, 825.
[20] S. Conesa-Boj, E. Russo-Averchi, A. Dalmau-Mallorqui, J. Trevino, E. F. Pecora, C. Forestiere, A. Handin, M. Ek, L. Zweifel, L. R. Wallenberg, D. Rüffer, M. Heiss, D. Troadec, L. Dal Negro, P. Caroff, A. Fontcuberta i Morral, *ACS Nano* **2012**, *6*, 10982.
[21] C.-Y. Chi, C.-C. Chang, S. Hu, T.-W. Yeh, S. B. Cronin, P. D. Dapkus, *Nano Lett.* **2013**, *13*, 2506.
[22] G. Tütüncüoglu, M. de la Mata, D. Deiana, H. Potts, F. Matteini, J. Arbiol, A. Fontcuberta i Morral, *Nanoscale* **2015**, *7*, 19453.
[23] P. Blanc, M. Heiss, C. Colombo, A. Dalmau Mallorquì, T. Saberi Safaei, P. Krogstrup, J. Nygård, A. Fontcuberta i Morral, *Int. J. Nanotechnol.* **2013**, *10*, 419.
[24] L. J. van der Pauw, *Philips Res. Reports* **1958**, *13*, 1.
[25] V. Y. Shevchenko, *Proceedings of the first international symposium on the physics and chemistry of II-V compounds*, Mogilany, **1980**, p. 15.
[26] W. Żdanowicz, K. Łukaszewicz, W. Trzebiatowski, *Bull. l'Académie Pol. des Sci., Série des Sci. Chim.* **1964**, *12*, 169.
[27] V. N. Yakimovich, V. A. Rubtsov, V. M. Trukhan, *Inorg. Mater.* **1996**, *32*, 705.
[28] G. Pangilinan, R. Sooryakumar, B. Chelluri, T. Y. Chang, *Phys. Rev. Lett.* **1989**, *62*, 551.
[29] J. Hanuza, A. Lemiec, J. Misiewicz, *Vib. Spectrosc.* **1998**, *17*, 93.
[30] G. Pangilinan, R. Sooryakumar, J. Misiewicz, *Phys. Rev. B* **1991**, *44*, 2582.
[31] J. Misiewicz, *Infrared Phys. Technol.* **1994**, *35*, 781.
[32] M. Iwami, K. Fujishima, K. Kawabe, *J. Phys. Soc. Japan* **1976**, *41*, 521.
[33] B. Sujak-Cyrul, B. Kolodka, J. Misiewicz, J. M. Pawlikowski, *J. Phys. Chem. Solids* **1982**, *43*, 1045.
[34] G. J. Scriven, A. W. R. Leitch, J. H. Neethling, V. V. Kozyrkov, V. J. Watters, *J. Cryst. Growth* **1997**, *170*, 813.
[35] S. F. Marenkin, N. S. Zhalilov, A. V. Mudryi, A. I. Patuk, I. A. Shakin, *Inorg. Mater.* **1992**, *28*, 1659.
[36] J. Szatkowski, K. Sierański, *Solid State Commun.* **1995**, *93*, 595.
[37] W.- J. Yin, Y. Yan, *J. Appl. Phys.* **2013**, *113*, 013708.
[38] B. Kołodka, J. Misiewicz, J. M. Pawlikowski, *Acta Phys. Pol. A* **1982**, *62*, 63.
[39] I. Åberg, G. Vescovi, D. Asoli, U. Naseem, J. P. Gilboy, C. Sundvall, A. Dahlgren, K. E. Svensson, N. Anttu, M. T. Björk, L. Samuelson, *IEEE J. Photovolt.* **2016**, *6*, 185.
[40] S. Gazibegovic, G. Badawy, T. L. J. Buckers, P. Leubner, J. Shen, F. K. de Vries, S. Koelling, L. P. Kouwenhoven, M. A. Verheijen, E. P. A. M. Bakkers, *Adv. Mater.* **2019**, https://doi.org/10.1002/adma.201808181.